Fabrication and Optical Modelling of Micro-Porous Membranes Index-Matched with Water for On-Line Sensing Applications

Roberta Lanfranco, Fabio Giavazzi, Tommaso Bellini, Emanuele Di Nicolò & Marco Buscaglia[*]

Dr. R. Lanfranco, Dr. F. Giavazzi, Prof. T. Bellini & Prof. M. Buscaglia
Dipartimento di Biotecnologie Mediche e Medicina Traslazionale, Università degli Studi di Milano, 20090 Segrate, Italy.
*marco.buscaglia@unimi.it
Current address of R. Lanfranco is Biological and Soft Systems, Cavendish Laboratory, University of Cambridge, JJ Thomson Avenue, Cambridge CB3 0HE, United Kingdom.

Dr. E. Di Nicolò
Solvay Specialty Polymers, 20021 Bollate, Italy.

Keywords: perfluoropolymers, label-free optical sensor, scattering phantom interface, molecular adsorption, membrane fouling.

Abstract
Membranes made of perfluorinated materials having refractive index close to that of water enable straightforward detection of water solutes at the interface, hence providing a novel sensing tool for fluidic systems. Here we report the production by non-solvent induced phase separation and characterization of microporous membranes made of Hyflon AD®, an amorphous copolymer of tetrafluoroethylene. We first studied their optical turbidity when soaked in liquids having different refractive index and interpreted the data with an optical model linking scattered light and structural features of the membrane. The average polymer and pore chord lengths obtained in this way scale with the filtering pore size measured by capillary flow porometry. We then investigated the optical response of the membranes when soaked in aqueous surfactant solutions and successfully interpreted the effects of the molecular absorption on the internal membrane surface by an extension of the model. Overall, our results show that index-matched membranes can be designed and produced to provide a simple optical detection of the composition of the soaking liquid or to monitor the initial stage of membrane fouling.

1. Introduction

Micro-porous membranes are widely used for several applications including filtering, separation, emulsification, reaction catalysis, analytical measurements, and fabric production.[1][2][3][4][5][6][7] Key membrane properties, such as filtering power, flow resistance and robustness, are determined by their internal structure. Moreover, degradation of membrane performance can be ascribed to structural modification or to incorporation of extrinsic particles or microorganisms that cause fouling or clogging. Therefore, various techniques have been proposed to characterize structural properties such as volume fraction of pores (porosity), pore size, pore shape distribution, specific surface area, and structural and chemical heterogeneity.[8][9] Most common characterization

approaches include flow measurements, gas adsorption, scattering of x-rays or light and electron microscopy.[10][11][12][13] For membranes with micron-scale structure, optical methods are particularly suitable and continuous technical improvements are proposed to obtain higher quality structural information. Optical investigation of membrane structures can be achieved by angle-resolved[14] or polarization-resolved[15] light scattering, by 3D optical reconstruction based on low coherence interferometry[16] or optical coherence tomography,[17] and by direct observation through confocal microscopy.[18]

Optical methods are non-destructive, non-contact and offer the opportunity to monitor the membrane status *in-situ*, while the membrane is used. For materials with negligible absorption of light, the complex porous structure provides a corresponding 3D spatial distribution of refractive index, which, in general, assumes different values for the solid part of the membrane and the porous regions filled by a liquid. A large mismatch between these two refractive indices produces opacity due to multiple scattering of light in all directions. Therefore, the membrane appears white and opaque when dried, due to the larger refractive index mismatch with air, and typically less opaque or translucent when wetted. In the single scattering regime, the amount of light scattered by the membrane in a given direction depends on the details of the inner structure. Several optical models have been proposed to link the structural features to the light scattering intensity.[19][20] However, the complexity of most approaches, the sensitivity to sample conditions and the requirement of highly specialized instruments have limited the widespread and general use of light scattering measurements for membrane structure characterization.

Partially fluorinated membranes, most commonly made of polyvinylidene fluoride (PVDF) or fully fluorinated membranes made by polytetrafluoroethylene (PTFE), have been extensively applied in several fields, from research applications to industrial processes, including water and waste water treatment, air filtration, membrane distillation, and pollutants removal.[21][22] They are preferred to other polymeric membranes for their outstanding properties such as the good chemical and thermal resistance. In addition, fully fluorinated membranes provide the peculiar optical feature of an

extraordinary low refractive index, which can reach values similar to that of water. However, most common PTFE membranes display a rather large scattering of light even in index-matching conditions because of embedded polycrystalline micro-structures with pronounced local birefringence and disordered orientation. Instead, perfluorinated materials made by Hyflon AD®, a class of commercial copolymers of tetrafluoroethylene (TFE) and 2,2,4 trifluoro, 5 trifluoromethoxy -1,3 dioxole (TTD),[23] provide a fully amorphous homogenous structure and a refractive index very close to that of water. Hyflon AD® is most commonly used as dense thin non-porous film for gas separation applications.[24][25] Previous use of Hyflon AD® in the membrane literature was mainly limited to membrane contactor applications, in particular providing a coating for PVDF membranes.[26][27][28] Micro-porous films made of Hyflon AD® were previously produced by phase separation to fabricate superhydrophobic films combining micro-patterning and enhanced surface roughness.[29]

Hyflon AD® 40 has 40 mol ratio of TTD and a refractive index n_m = 1.329, hence very close to that of water. An interface between an aqueous solution and this material provides a very low optical contrast that increases upon adhesion of other substances.[30] This peculiar feature enables the use of Hyflon AD® 40 in bios-sensing technologies. In the Reflective Phantom Interface method (RPI), prisms made of this material are exploited to build optical label-free biosensors to measure the interaction between molecular probes (e.g. antibodies or nucleic acids) immobilized on a planar surface and the corresponding target in solution through the increase of reflected light intensity.[31][32][33][34][35] Similarly, using the same approach, the bare surface of Hyflon AD®, without any functionalization, has been shown to retain different classes of molecules with different strength of adsorption.[36] The hydrophobic but slightly negatively charged surface favors the adsorption of molecular species with larger hydrophobic contact area and net positive charge. The same material has been previously used by the authors of the present work to fabricate micro-porous membranes providing very weak scattered light intensity when filled with water.[36] The adsorption of molecular compounds brought by the flow and binding to the inner membrane surface

yields a pronounced increase of scattered light intensity.[37] A microfluidic device embedding this membrane sensor in a cross-flow configuration has been proposed for continuous monitoring of environmental water pollution.[38]

In this work, we present the manufacturing and the characterization of micro-porous membranes made of Hyflon AD® 40 suitable for optical sensing. Hyflon AD® 40 was used as the sole component of the porous membranes, in order to exploit its amorphous structure and low refractive index. Our membranes become highly transparent when filled with water because of the very small difference of refractive index. **Figure 1** shows one of the membranes produced and characterized in this work when dried or soaked with ethanol or water. The main structural properties of the membranes were investigated by both standard membrane characterization techniques and through the study of the intensity of scattered light when the membranes are soaked with solutions having different refractive indices or containing molecular compounds adsorbing on the internal membrane surface. We developed a simple optical model derived from the random telegraph signal enabling to link the intensity of light scattered by the membrane to the structural characteristic size of membrane and pore regions. We tested this approach with commercial filters made of cellulose acetate (CA) and verified the proportionality between filtering pore size and optically-determined structural characteristic lengths. We propose this model as a general tool to investigate the internal structure of micro-porous membrane of Hyflon AD® in water and, more generally, for any kind of membrane close to index matching condition with the filling solution. Hyflon AD® membranes with selected structural features can be used as optical sensors of water contamination or as a tool for quantitative monitoring of the initial stage of fouling, a common phenomenon due to the deposition of foulants on the internal and external surface of porous membranes and the subsequent clogging of pores. In fact, to prevent loss of functionality and performances it would be desirable to monitor the membrane status and in particular to quantify the deposition of such foulants at an early stage during the use.

2. Results & Discussions

2.1. Fabrication and selection of Hyflon AD membranes

The production of micro-porous membranes made of Hyflon AD® was performed by Non-solvent Induced Phase Separation (NIPS) technique, which is the most common method for the fabrication of commercial flat sheet membranes and hollow fibers.[39] Tests to select the suitable conditions for casting were performed with different solvents and polymer amounts (see S1). The solvents HFE 7100, HFE 7300 and perfluoroctane dissolved quite easily Hyflon AD® and showed a viscous behaviour at room temperature suitable for casting in a range of concentrations from 12% to 20% wt. Therefore, these solvents were tested for membrane fabrication and we were able to obtain membranes in all cases. However, at visual inspection, the membranes produced using perfluoroctane and 1,3-bis(trifluoromethyl)benzene as non-solvent had a white, wrinkly and non-homogeneous appearance likely indicating a too slow solvent exchange process. In contrast, the membranes made with HFE 7100 and HFE 7300 had a more homogenous appearance and transparency when soaked with ethanol and hence we explored different preparation conditions using these two solvents (Table S2). We observed a variety of different morphologies, both for the external surface and the internal structure of the membranes. As model systems to study the optical response of the Hyflon AD® membranes we selected three samples produced by HFE 7100 (membrane 3, 5 and 7 in Table S2) and one sample made with HFE 7300 for comparison (membrane 22). These membranes appeared largely homogenous by visual inspection, while they showed different structures by SEM, hence providing a suitable benchmark to test the optical model. In **Figure 2** we show SEM images of the selected membranes. The size, the spatial distribution and the interconnection of the pore regions differed considerably depending on the preparation conditions, which are reported in **Table 1**. Sample 3 (and in general all samples without cyclohexanone) showed a quite tight morphology with a dense upper surface and low (gravimetric) porosity indicating a slow coagulation process.[40] In particular, from inspection of SEM images, samples 5 and 7 showed pores that appeared more interconnected than those of other samples. Besides, the overall porosity of these two samples was also larger (Table 1). In general, we

observed that, increasing the amount of acetone in the coagulation bath, the membrane porosity tended to become larger. The addition of 5% wt of the non solvent cycloexanone in the casting solution prepared with HFE 7100, as for membrane 5 and 7, yielded to a larger porosity of about 70%-75%, more uniform morphology and larger thickness. This could be explained by a faster coagulation induced by the presence of a non-solvent in the dope solution. Since the manufacturing was accomplished with the final scope of sensing application, a larger value of porosity was considered more preferable in order to decrease the flow resistance across the items and more easily wet the pores of the hydrophobic membrane. Moreover, cyclohexanone decreased the boiling point of the casting solution avoiding the formation of bubbles on the surface of the casted film and reduced the skin formation on the air side. To this aim also the casting temperature at 10°C helped in keeping the solution mixture significantly below the boiling point. Another important factor affecting the exploitability of these membranes is their chemical and physical stability. The membranes made with HFE 7100 were stable for several months at room temperature, whereas the appearance of some of the membranes produced using HFE 7300 changed over time when stored in water/alcohol at room temperature. Moreover, these membranes also showed a larger variability of porosity for repeated productions in the same conditions. We attribute this instability to the amount of residual solvent trapped within the membranes, which could have plasticised the polymer structure and eventually lead to collapse of some pores, a phenomenon already observed for Hyflon AD®.[41] Samples made with a small amount of cyclohexanone exhibited a lower amount of residual solvent estimated by TGA measurements (Figure S3), compared to membrane produced with pure HFE 7100 and HFE 7300. This could be explained by an increase of affinity with non-solvent baths, which enabled a more effective removal of the solvent during the phase inversion.

2.2. Optical turbidity of index-matched membranes

The opacity of a porous membrane soaked with a liquid depends on both its structure and refractive index. If the refractive index of the membrane material and that of the soaking liquid are close enough, the membrane becomes more transparent and the residual opacity depends on the inner structure of the membrane. We measured the optical turbidity τ of the newly fabricated membranes made of Hyflon AD® varying the refractive index mismatch with the solution. We soaked them with water and progressively added ethanol to change the solvent's refractive index n_s. As shown in **Figure 3a**, all membranes showed a continuous increase of turbidity with n_s. The measured behaviour is well fitted by parabolic functions with a minimum corresponding to full transparency ($\tau \approx 0$) for n_s = 1.329±0.001, indicating the matching with the refractive index n_m of Hyflon AD®. In the case of membranes 5 and 7, we observed a large increase of τ for rather small increments of n_s. In contrast, membranes 3 and 22 showed a much weaker dependence on the solution refractive index. The different optical response is ascribed to structural differences of the membranes, which can be quantified in different ways. In fact, parameters addressing both the quantity and the size of the scattering elements are needed to model the optical response. Here we propose a simple approach based only on two structural parameters: the volume fraction of liquid ϕ, or porosity, and the characteristic size m of the membrane structural elements. The value of the porosity ϕ was measured by comparing the weight of dried and soaked membranes. As reported in **Table 2**, although larger values of ϕ seem roughly to correspond to larger turbidity in Figure 3a, the absence of a clear scaling between τ and ϕ confirms that the membrane opacity also depends on other parameters related to its internal structure, which can be estimated through a suitable optical model.

As a benchmark, we compared the turbidity of Hyflon AD® membranes with that of CA filtering membranes. We performed measurements on commercial CA membranes (Sartorius) with different nominal filtering pore size d_{pore}: 0.45 μm, 0.65 μm and 5 μm. As confirmed by independent measurements, these CA membranes have similar porosity (Table 2). Cellulose acetate has a refractive index n_m = 1.475, much higher than that of water. Therefore, to progressively change the refractive index inside the measuring cell and achieve index matching conditions, we soaked CA

filters with mixtures of p-cymene (n_s = 1.4905) and isopropyl alcohol (n_s = 1.3776). **Figure 3b** reports the turbidity measured for the three CA filters as a function of the solution refractive index. All membranes showed a minimum of τ for n_s = 1.475 ±0.001 and a quadratic dependence of τ on n_s, similarly to Hyflon AD® membranes. The turbidity also increased with the nominal filtering pore size d_{pore} of the membranes. Considering the turbidity dependence on the refractive index mismatch between membrane and solution $\Delta n = n_s - n_m$, for the same value of Δn the studied CA membranes showed a turbidity similar to those of membranes 3 and 22 and much smaller than that of membrane 5 and 7.

A general relation linking the optical properties to the internal structure of a membrane can be rather complicated. However, in particular conditions simplified relations can be derived to accurately account for the turbidity and the intensity of scattered light. A special case is provided by membranes made of non-absorbing and homogenous material with refractive index close enough to that of the soaking liquid. In this case, the scattering is rather weak, and the calculation becomes simpler assuming that neither the amplitude nor the phase of the incident radiation changes significantly crossing the membrane. These assumptions correspond to the so-called Rayleigh-Gans (RG) approximation.[19] In this regime, it is necessary to compute the total contribution of all the elementary scattering elements in the porous material. To achieve this, we adopted a description of the membrane structure only based on two characteristic lengths: the average chord lengths inside the solution regions (*s*) and the solid parts of the membrane (*m*) obtained by piercing the membrane with straight lines with random orientation. Considering all the possible rays crossing the membrane, *s* and *m* represent the average lengths of the ray segments in the void and solid regions, respectively, as described in **Figure 4a**. This approach corresponds to treat the fluctuations of dielectric constant experienced by a light ray passing through the membrane as a Random Telegraph Signal (RTS). A similar approach was first proposed by Debye to model the small angle x-ray scattering from porous media.[42] The dielectric constant ε evaluated on a line with random orientation crossing the membrane undergoes sharp transitions between two values, those of

solution (ε_s) and membrane (ε_m), with average distance s and m between two consecutive transitions, respectively (**Figure 4b**). In this framework, the expression for the spatial correlation function of the dielectric constant fluctuations $\langle \delta\varepsilon(r)\delta\varepsilon(r+dr)\rangle$ is derived by the conditional probabilities of starting from a medium (membrane or solution) at position r and finding the same or the other medium at a distance dr. The calculation can be performed considering an equivalent two-state kinetic model, where the time coordinate is replaced by the space r and the characteristic rates are $1/m$ and $1/s$, respectively (**Figure 4c**). The model provides a correlation function decaying exponentially with a space constant $\gamma = (1/m+1/s)$:

$$\langle \boldsymbol{\delta\varepsilon(r)\delta\varepsilon(r+dr)}\rangle = \frac{\boldsymbol{ms}}{\boldsymbol{(m+s)^2}}\boldsymbol{(\varepsilon_s-\varepsilon_m)^2 e^{-\gamma r}} \quad (1)$$

From the Fourier transform of Equation (1) the intensity of scattered light at distance R in the direction indicated by the scattering vector q and the turbidity τ are given by (see section S5 in SI):

$$\boldsymbol{I_s(q,R) = C(R)N_0^2\frac{1-\phi}{m}\frac{k^4}{(q^2+\gamma^2)^2}} \quad (2)$$

$$\boldsymbol{\tau = N_0^2\frac{1-\phi}{m}\frac{k^4}{\gamma^2(\gamma^2+4k^2)}} \quad (3)$$

In Equation (2), $C(R) = I_0V/(4\pi R^2)$ accounts for the instrumental parameters. In both equations, the volume fraction ϕ of solution, or porosity, is given by [43] $\boldsymbol{\phi = \frac{s}{s+m}}$ and $\boldsymbol{N_0 = \frac{n_s^2-n_m^2}{(n_s^2-n_m^2)\phi+n_m^2}}$. These equations are valid for any value of the refractive indices and for $0 < \phi < 1$, provided the validity of the RG approximation. In the case of porous systems with values of n_s and n_m similar enough, $\boldsymbol{N_0}$ can be further approximated considering its expansion in $\Delta n = n_s - n_m$. This leads to a simpler expression that does not depend on the structural parameters ϕ or s:

$$\boldsymbol{N_0^2 \approx \left(\frac{2\Delta n}{n_m}\right)^2} \quad (4)$$

This approximation is valid for $(n_s^2 - n_m^2)/\, n_m^2 << 1$. As an example, for n_m close to the refractive index of water $n_w = 1.333$, as in the case of the Hyflon AD® membranes, Equation (4) leads to a relative error $(N^2/N_0^2 - 1)$ on the scattered intensity or the turbidity lower than 1% for $n_s < 1.338$ or

lower than 5% for $n_s < 1.355$. In these quasi-index matching conditions, both the scattered light and the turbidity simply scale with Δn^2, and all the parameters related to the structural features of the membrane can be grouped in the remaining factors, obtained as $F_I = I_s / (CN_0^2)$ or $F_T = \tau / N_0^2$, respectively, which are independent from the refractive index. **Figure 5** reports the behaviour of these factors for different values of m and ϕ. At constant ϕ, the scattered intensity at fixed angle $\theta = 30°$ shows a maximum value as a function of m, which shifts from $m \approx 1$ μm for very low values of ϕ to $m << 1$ μm for larger ϕ (Figure 5a). After the peak, I_s decreases proportionally to m^{-1}. In contrast, the turbidity, which represents the total scattered light in all directions, continuously increases with m but the scaling exponent changes from $\tau \propto m^3$ to $\tau \propto m$ in correspondence of the peak of I_s (Figure 5c). At constant m, as expected, both F_I and F_T tend to decrease for values of ϕ close to 0 or close to 1 (Figure 5b and 5d).

Equation (3) enables the investigation of the membranes structure by means of the turbidity measurements as a function of Δn reported in Figure 3. The structural parameters m or s can be straightforwardly estimated from the quadratic dependence of τ on Δn for CA and Hyflon AD® membranes. The porosity ϕ was constrained to the value measured independently (Table 2). This in practice corresponds to fix the ratio between m and s. The obtained values of m and s are reported in Table 2. In the case of CA membranes, both parameters scale with the nominal filtering pore size d_{pore}, although they are larger. In order to confirm this behaviour, we independently measured d_{pore} of CA membranes by capillary flow porometry (Table S3) and obtained values consistent with the nominal pore size. Remarkably, m is repeatedly found to be about a factor of two larger than d_{pore}. In contrast, the values of s are much larger than the pore size, roughly by a factor of 10. In fact, d_{pore} represents the smallest diameter encountered along the through pores, whereas s indicates the average length of the chords connecting two points on the membrane in the solution space, and, therefore, it is always larger than d_{pore}.

We applied the same analysis of the turbidity to the Hyflon AD® membranes and found a range of values for m and s similar to those obtained for CA filters (Table 2). In this case, reliable measurements of d_{pore} by capillary flow porometry were obtained for membrane 7 only. Remarkably, as shown in **Figure 6** (brown symbols), the scaling between m and d_{pore} for this membrane was the same observed in the CA membranes. In contrast, the obtained value of s was similar to that measured for the CA5 membrane, which has a smaller pore size than membrane 7. A direct determination of d_{pore} by capillary flow porometry for membranes 3, 5 and 22 was not possible because of the closed pore structure of one side of the membranes. Differently, the optical measurements are not affected by this limitation. Therefore, assuming the same scaling observed for the CA membranes and membrane 7, d_{pore} for the other membranes was estimated from m by interpolation of the data in Table 2 (open diamonds in Figure 6). Similarly to membrane 7, also the other membranes showed smaller values of the s parameter in comparison with CA membranes, hence indicating a smaller characteristic size of the open volume inside the membrane, which provides a direct contribution to the optical turbidity.

Despite the different materials, morphology and porosity, the simple optical analysis proposed in this study enables to extract consistent parameters related to the internal structure of the membranes complementary to pore size and porosity. Moreover, the optical investigation enables the structural characterization of membranes with very low porosity and with one closed surface. The relation between the structure, the pore size and the parameters m and s can be further investigated by simulating 3D structures with variable open volume size and through pore diameter, as shown in section S6 of SI. From the analysis of different simulated structures (Figure S5), the ratio of the average chord lengths is confirmed to provide an estimate of the porosity ϕ, as $\phi = (m/s + 1)^{-1}$. The pore size d_{pore} is defined as the minimum diameter of all the apertures that a fluid has to go through in order to move across the membrane, from one side to the other. Therefore, the larger values of s and m relative to d_{pore} indicate the presence of rather narrow openings separating much larger cavities in the inner structure of the membranes. A similar behaviour can be obtained for example

from a simulated structure rich of walls with narrow holes (Figure S5f). More realistic representations of the membrane structure should have random distribution of size and position of the inner structural elements. However, even in this case, *s* and *m* would represent average values of the chord lengths, whereas d_{pore} would be given by the smaller minimum aperture size.

The RTS model proposed in this work is arguably the simplest approach to predict the intensity of light scattered by a micro-porous membrane properly taking into account the porosity ϕ. Simpler models can be derived considering a collection of independent scattering objects.[36] However, in this case, the void fraction is a complex parameter linked to the size, shape and space distributions of the objects. Because of its simplicity and robustness, the RTS model provides a general solution that neglects structural details others than the mean chord lengths of membrane and solution regions. Therefore, it is based on a strongly approximated description of the internal membrane structure. In particular, it has been shown by small angle light scattering that filtering membranes can display quasi-periodic features and a fractal structure on the micron scale.[14] The simple RTS model does not account for these behaviours since the *q*-dependence of the scattered intensity described by Equation (2) is given by a squared Lorentzian function, commonly found in RG models of independent scatterers.[19] Extended random telegraph models that include fractal distributions have been proposed to describe burst noise in defective operational amplifiers and ion currents through a cell membrane.[44] This approach could be exploited in future works to further extend the RTS model to account for fractal membrane structures.

2.3. Optical response of Hyflon AD membranes upon adsorption

Microporous membranes with refractive index close to that of the solution provide a pronounced increase of light scattering intensity upon adsorption of molecular compounds onto the inner surface. In particular, membranes made of Hyflon AD® are almost index-matched with water, hence they can be exploited as optical sensor for water contaminants.[38] The adsorption strength and kinetics

on Hyflon AD® depends on both the hydrophobic contact area and the net charge of the compounds.[36] Among other types of molecules, cationic surfactants spontaneously adsorb on Hyflon AD® and fully cover the interface with water at large concentrations. To some extent, the optical response of these membrane sensors is expected to depend on the specific internal structure. We tested the optical response upon adsorption for membranes 5 and 7, those with the largest porosity and pore size but with different inner structure, as indicated by SEM images (Figure 2) and by optical analysis (Table 2). We immersed membranes 5 and 7 in 1 ml of a solution containing increasing concentration of cationic surfactant benzyldimethylstearylammonium chloride monohydrate (SBSAC) up to 1.2 mM. The intensity of scattered light I_s measured at 30° and normalized to the value I_{s0} measured in absence of surfactant is reported in **Figure 7a** as a function of the surfactant concentration C_s. Both membranes displayed an increase of scattered light intensity, although with different behaviours. Membrane 7 showed a continuous increase up to about 20% of relative scattered intensity, whereas membrane 5 provided a rather sharp minimum at about 100 μM followed by a larger increase up to about 60% of the signal. The data points displaying a monotonic increase with C_s were fitted with a Langmuir isotherm curve, from which we obtained the concentration of half surface coverage $C_{1/2}$ of 0.53 mM and 1.34 mM for membrane 5 and 7, respectively.

The RTS model extended to three layers provides a theoretical framework to interpret the scattered intensity of Hyflon AD® membranes upon adsorption. The adhesion of compounds with refractive index different from those of membrane and solution onto the internal surface of the membrane modifies the distribution of dielectric constant $\delta\varepsilon(r)$ inside the porous medium, hence altering the scattering of light. In the framework of the RTS model, the formation of a layer with refractive index n_h and thickness h, much smaller than the wavelength, at the inner interface between the membrane and the solution can be accounted as an additional step-like change of dielectric constant. A light ray crossing the membrane volume passes through the thin layer at each membrane-solution and solution-membrane transition (**Figure 4d**). As for the two-state RTS model

described above, the autocorrelation function of $\delta\varepsilon(r)$ is derived from an equivalent four-state kinetic system continuously cycling through the sequence of dielectric constant states $\varepsilon_m \rightarrow \varepsilon_h \rightarrow \varepsilon_s \rightarrow \varepsilon_h \rightarrow \varepsilon_m \ldots$ (**Figure 4e**). Similarly to the calculation performed for the two-state RTS model, the transition rates are given by $1/m$, $1/s$ and $1/h$, where h is much smaller than m and s. With this approximation, only two non-degenerate rates are obtained from the model: $\gamma = (1/m+1/s)$ and $\gamma_h = 1/h$. Therefore, the spatial correlation function of the dielectric constant fluctuations $\langle \delta\varepsilon(r)\delta\varepsilon(r+dr)\rangle$ is written as the sum of two exponential decays with rates γ and γ_h:

$$\boldsymbol{\langle \delta\varepsilon(r)\delta\varepsilon(r+dr)\rangle = (a_0 - a_h)e^{-\gamma_h r} + a_h e^{-\gamma r}}. \quad (5)$$

where a_o and a_h are obtained considering the limit for $dr = 0$, and for $h << dr_h << m$ and s, (see S5 in SI). The intensity of scattered light and the turbidity can be recovered from the Fourier transform of Equation (5). Remarkably, this approach can be generalized to systems composed by any number of material layers with different values of dielectric constant. In case considered here, we computed the ratio between the scattered intensity I_s in the presence of the layer h and the intensity I_{s0} scattered by the bare membrane ($h = 0$) for $n_s \approx n_m$:

$$\boldsymbol{\frac{I_S}{I_{s0}} = 1 + h\gamma(1-2\phi)N_1 + 2h^4(\gamma^2+q^2)^2 N_1^2} \quad (6)$$

where

$$\boldsymbol{N_1 = \frac{(n_h^2 - n_s^2)}{(n_s^2 - n_m^2)} \approx \frac{1}{N_0}\left(\frac{n_h^2}{n_s^2} - 1\right)} \quad (7)$$

According to Equation (6), the linear term in h is negative for $\phi > 0.5$ if $n_s > n_m$, hence providing an initial small decrease of the scattered light intensity with the growth of parameter h followed by an increase as h^4.

Figure 7b report I_s/I_{s0} computed through Equation (6) using the parameters extracted for membrane 5 and 7, respectively (Table 2). The amount of surfactant adsorbed at the internal membrane surface is modelled as an effective refractive index n_h of a layer with thickness h separating the membrane and solution volumes. The values of h were chosen in order to reproduce the values of I_s/I_{s0} reported

in Figure 7a, yielding to 18.5 nm and 14 nm and for membrane 5 and 7, respectively. As shown in the plot, for membrane 5 the model predicts a shallow initial decrease of the scattering intensity as a function of n_h, qualitatively similar to what was measured experimentally, although the depth of the minimum in Figure 7b (inset) is much less pronounced. In general, the depth of the minimum predicted by Equation (6) scales with γ^2 for $q >> \gamma$ at constant ϕ, hence it is more pronounced for smaller m and s, as in the case of membrane 5. In this condition, the adsorbed layer basically affects the mean refractive index of the coated membrane structure and provides a better matching with the filling solution. Similarly, a local minimum of scattered intensity at the initial stage of coating was previously observed for a system of dispersed nanoparticles index matched with water.[45]

The analysis yields characteristic sizes h of the surfactant layer significantly larger than the expected size of a monolayer of SBSAC, which is about 2.4 nm.[36] A correction of about $\pi/2$ can be applied to consider that the chord length h of the RTS model corresponds to the average length of a segment crossing a layer with thickness h_0 with random 3D orientation, and therefore $h > h_0$. This correction leads to a layer thickness h_0 in the range of 8-12 nm, hence still larger than the molecule size. The discrepancy with the size of SBSAC molecule suggests that the adsorption on the internal membrane surface yields to the formation of surface structures of surfactant, like multi-layers or surface micelles, instead of a monolayer.[46][47][48] A comparison between the measured values of $C_{1/2}$ for adsorption and the estimated membrane surface supports this interpretation.

Previous measurements of adsorption of SBSAC on a planar surface of Hyflon AD® has led to equilibrium dissociation constants as small as 160 nM. Therefore, the much larger values of $C_{1/2}$ for adsorption on the membrane is ascribed to mass limitation effect due to a large number of available binding sites N_s.[36] In these conditions, $C_{1/2}$ is expected to depend on the total concentration of binding sites as $C_{1/2} \approx N_s/(2V_tN_a)$, where V_t = 1 ml is the total sample volume and N_a is the Avogadro number. The corresponding total adsorption surface that can be potentially covered by a monolayer of SBSAC molecules is $S_a = N_sA_{mol}$, where $A_{mol} \approx 0.7$ nm^2 is the adsorption area per molecule.[36] The value of S_a for membranes 5 and 7 is 0.44 m^2 and 1.1 m^2, respectively. These

values can be compared with the internal surface S of the membrane estimated from the structural parameters. Interestingly, the surface to volume ratio S/V of the membrane can be estimated from the chord lengths s and m obtained from optical analysis (Table 2). Considering a 3D medium containing figures of any shape with total volume of the figures V_m, and throwing lines of length l many times at random, it can be demonstrated that $S/V_m = 4c_{cross}/(lc_{in})$, where c_{in} is the average number of line ends found inside the figures and c_{cross} is the average number of intersections of the figures surface.[49] This result can be straightforwardly extended to the case of very long segments resembling the rays of the RTS optical model. In this case, the probability of finding one line end, alias one random point, inside the membrane material is simply given by $1-\phi = \mathrm{m}/(\mathrm{m+s})$. Therefore, considering a line longer than the correlation lengths of the structure, $c_{in} = 2m/(m+s)$. The number of intersections can be derived by the average chord lengths considering that in average the line undergoes two transitions after a length $m+s$, hence $c_{cross} = 2l/(m+s)$. Accordingly, for l long enough, $S/V_m=4/m$, and from $V_m = V(1-\phi)$ we obtain $S/V = 4(1-\phi)/\mathrm{m} = 4/(\mathrm{m+s})$. Therefore, the surface to volume ratio of membrane 5 and 7 consistent with the values reported in Table 2 are 0.17 μm^{-1} and 0.07 μm^{-1}. For a membrane fragment of 0.5 cm^2 and a thickness of about 100 μm, these values correspond to a total membrane surface $S = 8.5\cdot10^{-4}$ m^2 and $S = 3.5\cdot10^{-4}$ m^2, respectively. Thus, the internal surface of the membrane is much smaller than that corresponding to a monolayer of surfactant. Therefore, the large values of both $C_{1/2}$ and h are ascribed to the formation of thicker surfactant structures on the membrane surface.

3. Conclusions

Microporous membranes with refractive index similar to that of water provide a tool to monitor adsorption of molecular pollutants or foulants by measuring a light scattering intensity signal. We showed that perfluorinated membranes index matched with water can be produced by NIPS technique obtaining different porosity and structures. They represent a new class of membranes combining filtering and sensing capabilities. They retain a fully amorphous polymer structure and

combine all the advantages of PTFE (in particular chemical and thermal stability) with a homogenous optical structure, hence enabling a straightforward optical characterization and inspection of the membrane. When used in combination with filtering of aqueous solutions, they offer the advantage of real time quantification of the cleanliness condition of the inner membrane surface at nanometer scale, hence enabling to detect the initial stage of fouling. In turn, as optical sensors they embed size exclusion filtering capability. The condition of index matching with the solution also enables simplified theoretical modelling of the light scattering signal. We have developed a simple model derived from the random telegraph signal. The model accounts for two characteristic lengths to describe the two-component internal optical structure made of membrane and solution. The effect of an adsorbed layer placed at the membrane-solution interface is modelled as a third material, alias a third layer, of the random telegraph model. Through this model, we showed that the analysis of the optical response of index-matched membranes upon changes of solution refractive index or content of adsorbant molecules provides a general tool to access structural information complementary to those obtained from other widely used membrane characterization methods. Surprisingly, the dependence of membrane turbidity on the solution refractive index is found to scale with the filtering pore size, although this indicates the minimum diameter of the apertures, whereas the scattered light depends on the average size of the inner membrane volumes. Additionally, the modelling of the optical response to molecular adsorption enables the quantification of the effective thickness of a layer formed on the internal membrane surface. Overall, index-matched membranes offer optical sensing properties that depend on their internal structure. Therefore, the production of membranes with tailored features through suitable modelling and characterization tools enables their full exploitation in a wide range of potential applications.

4. Experimental Section

Materials: Hyflon AD® 40 and Galden SV90, a low molecular weight perfluoropolyether with a boiling point of 90°C, was gently provided by Solvay Specialty Polymers, Bollate (MI). HFE-7300

[$C_2F_5CF(OCH_3)CF(CF_3)_2$] and HFE-7100 [$CH_3OCF_2CF(CF_3)_2$] were both purchased from 3M. CA membranes were purchased from Sartorius. Perfluorooctane [C_8F_{18}], ethanol, acetone, and 1,3-bis(trifluoromethyl)benzene used for the coagulation bath, and isopropyl alcohol used to test the membranes were purchased from Sigma Aldrich. Cyclohexanone, used as a non-solvent in the casting formulation, and P-cymene were purchased from Sigma Aldrich.

Membrane production: Hyflon AD® membranes were produced using NIPS method. Preliminarily, the solubility of Hyflon AD® was tested at different temperature in different solvents in order to find suitable conditions of polymer viscosity for casting (see SI). The casting solutions for the production of the membrane were prepared dissolving the polymer in the solvents under stirring for 24 hours at room temperature and then ultra-sonicated for 30 minutes to eliminate bubbles. A small amount of cyclohexanone was added occasionally to the casting solution in order to accelerate the precipitation of the nascent membrane. The solution was casted on a glass plate using an automatic film applicator (Elcometer 4340) with 250 μm gap. Different compositions of coagulation bath were explored: pure ethanol, a mixture of ethanol/acetone 7:3 vol., a mixture of ethanol/acetone 1:1 vol and pure 1,3-bis(trifluoromethyl)benzene. All the chemicals were used without any further purification. The coagulation process lasted for 15 minutes. The casting solutions were all kept at 25°C; the coagulation bath was set at 25°C or 10°C. All samples except those soaked with ethanol underwent to a washing step of pure ethanol for 10 minutes at room temperature in order to fully extract the residual solvents. For some samples, an additional step to open membrane surfaces was performed by soaking the membrane for 15 minutes with different mixture of HFE7100 and ethanol. Finally, all the samples were stored in a 30%-70% vol of ethanol-water.

Membrane characterization: Newly Hyflon AD® membranes were characterized with the following standard methods: thickness, gravimetric porosity, pore size, scanning electron microscopy imaging and thermal gravimetric analysis. The details of these characterizations are reported in section S2 of SI. Moreover, we performed a novel non-invasive optical study to

understand the internal morphology of the porous medium. A more exhaustive explanation of the system used for this technique is reported in S4 of SI.

Supporting Information
Supporting Information is available from the Wiley Online Library or from the author.

Acknowledgements
This project has received funding from the European Union's Seventh Framework Programme (FP7) for Research, Technological Development and Demonstration through the NAPES project (grant agreement no. 604241).

References

[1] D. K. Wang, R. A. Bauer, K. Yan, I. A. Mergos, Z. Yang, Y. Zhou, H. Verweij, *Adv. Mater. Interfaces* **2019**, *6*, 1801273.

[2] E. Piacentini, E. Drioli, L. Giorno, *J. Memb. Sci.* **2014**, *468*, 410.

[3] Y. Wei, H. Qi, X. Gong, S. Zhao, *Adv. Mater. Interfaces* **2018**, *5*, 1800576.

[4] H. Ruan, J. Liao, R. Tan, J. Pan, A. Sotto, C. Gao, J. Shen, *Adv. Mater. Interfaces* **2018**, *5*, 1800909.

[5] S. Feng, Z. Zhong, Y. Wang, W. Xing, E. Drioli, *J. Memb. Sci.* **2018**, *549*, 332.

[6] A. Gugliuzza, E. Drioli, *J. Memb. Sci.* **2013**, *446*, 350.

[7] X. Wang, Y. Zhao, E. Tian, J. Li, Y. Ren, *Adv. Mater. Interfaces* **2018**, *5*, 1701427.

[8] D. M. Smith, D.-W. Hua, W. L. Earl, *MRS Bull.* **1994**, *19*, 44.

[9] S. Nakao, *J. Memb. Sci.* **1994**, *96*, 131.

[10] C. Hörenz, C. Pietsch, A. S. Goldmann, C. Barner-Kowollik, F. H. Schacher, *Adv. Mater. Interfaces* **2015**, *2*, 1500042.

[11] A. Hernandez, *J. Memb. Sci.* **1996**, *112*, 1.

[12] K. Kaneko, *J. Memb. Sci.* **1994**, *96*, 59.

[13] L. F. Gate, *J. Phys. D. Appl. Phys.* **1972**, *5*, 327.

[14] L. Cipelletti, M. Carpineti, M. Giglio, *Langmuir* **1996**, *12*, 6446.

[15] Y. Wyart, G. Georges, C. Deumié, C. Amra, P. Moulin, *J. Memb. Sci.* **2008**, *318*, 145.

[16] C. Mujat, L. Denney, A. Dogariu, *MRS Proc.* **2000**, *613*, E6.10.1.

[17] L. Fortunato, S. Bucs, R. V. Linares, C. Cali, J. S. Vrouwenvelder, T. Leiknes, *J. Memb. Sci.* **2017**, *524*, 673.

[18] A. Ley, P. Altschuh, V. Thom, M. Selzer, B. Nestler, P. Vana, *J. Memb. Sci.* **2018**, *564*, 543.

[19] H. C. van de Hulst, *Light Scattering by Small Particles*, Dover, New York, **1957**.

[20] C. M. Sorensen, *Aerosol Sci. Technol.* **2001**, *35*, 648.

[21] G. Kang, Y. Cao, *J. Memb. Sci.* **2014**, *463*, 145.

[22] F. Liu, B. Yi, D. Xing, J. Yu, H. Zhang, *J. Memb. Sci.* **2003**, *212*, 213.

[23] "No Title," can be found under https://www.solvay.com/en/brands/hyflon-ad, **n.d.**

[24] T. C. Merkel, I. Pinnau, R. Prabhakar, B. D. Freeman, in *Mater. Sci. Membr. Gas Vap. Sep.*, John Wiley & Sons, Ltd, Chichester, UK, **2006**, pp. 251–270.

[25] Y. Okamoto, H. Zhang, F. Mikes, Y. Koike, Z. He, T. C. Merkel, *J. Memb. Sci.* **2014**, *471*, 412.

[26] A. Gugliuzza, E. Drioli, *J. Memb. Sci.* **2007**, *300*, 51.

[27] T. A. Jalal, N. M. S. Bettahalli, N. L. Le, S. P. Nunes, *Ind. Eng. Chem. Res.* **2015**, *54*, 11180.

[28] D. Tong, X. Wang, M. Ali, C. Q. Lan, Y. Wang, E. Drioli, Z. Wang, Z. Cui, *Sep. Purif. Technol.* **2016**, *157*, 1.

[29] L. Vogelaar, R. G. H. Lammertink, M. Wessling, *Langmuir* **2006**, *22*, 3125.

[30] R. Lanfranco, M. Buscaglia, in *Ref. Modul. Mater. Sci. Mater. Eng.*, Elsevier, **2016**.

[31] F. Giavazzi, M. Salina, R. Cerbino, M. Bassi, D. Prosperi, E. Ceccarello, F. Damin, L. Sola, M. Rusnati, M. Chiari, B. Chini, T. Bellini, M. Buscaglia, *Proc. Natl. Acad. Sci.* **2013**, *110*, 9350.

[32] F. Giavazzi, M. Salina, E. Ceccarello, A. Ilacqua, F. Damin, L. Sola, M. Chiari, B. Chini, R. Cerbino, T. Bellini, M. Buscaglia, *Biosens. Bioelectron.* **2014**, *58*, 395.

[33] M. Salina, F. Giavazzi, E. Ceccarello, F. Damin, M. Chiari, M. Ciuffo, G. P. Accotto, M. Buscaglia, *Sensors Actuators B Chem.* **2016**, *223*, 957.

[34] G. Tagliabue, V. Faoro, S. Rizzo, D. Sblattero, A. Saccani, G. Riccio, T. Bellini, M. Salina, M. Buscaglia, A. Marcello, *Biochem. Biophys. Res. Commun.* **2017**, *492*, 558.

[35] G. Nava, E. Ceccarello, F. Giavazzi, M. Salina, F. Damin, M. Chiari, M. Buscaglia, T. Bellini, G. Zanchetta, *Phys. Chem. Chem. Phys.* **2016**, *18*, 13395.

[36] R. Lanfranco, F. Giavazzi, M. Salina, G. Tagliabue, E. Di Nicolò, T. Bellini, M. Buscaglia, *Phys. Rev. Appl.* **2016**, *5*, 054012.

[37] G. Zanchetta, R. Lanfranco, F. Giavazzi, T. Bellini, M. Buscaglia, *Nanophotonics* **2017**, *6*, DOI 10.1515/nanoph-2016-0158.

[38] R. Lanfranco, J. Saez, E. Di Nicolò, F. Benito-Lopez, M. Buscaglia, *Sensors Actuators B Chem.* **2018**, *257*, 924.

[39] F. Tasselli, in *Encycl. Membr.*, Springer Berlin Heidelberg, Berlin, Heidelberg, **2014**, pp. 1–3.

[40] R. W. Baker, *Membrane Technology and Applications*, John Wiley & Sons, Ltd, Chichester, UK, **2012**.

[41] M. Macchione, J. C. Jansen, G. De Luca, E. Tocci, M. Longeri, E. Drioli, *Polymer (Guildf).* **2007**, *48*, 2619.

[42] P. Debye, H. R. Anderson, H. Brumberger, *J. Appl. Phys.* **1957**, *28*, 679.

[43] A. V. Malinka, *J. Quant. Spectrosc. Radiat. Transf.* **2014**, *141*, 14.

[44] L. S. Liebovitch, *Ann. Biomed. Eng.* **1988**, *16*, 483.

[45] D. Prosperi, C. Morasso, F. Mantegazza, M. Buscaglia, L. Hough, T. Bellini, *Small* **2006**, *2*, 1060.

[46] R. Atkin, V. S. J. Craig, E. J. Wanless, S. Biggs, *Adv. Colloid Interface Sci.* **2003**, *103*, 219.

[47] S. Paria, K. C. Khilar, *Adv. Colloid Interface Sci.* **2004**, *110*, 75.

[48] S. O. Nielsen, G. Srinivas, C. F. Lopez, M. L. Klein, *Phys. Rev. Lett.* **2005**, *94*, 228301.

[49] H. W. Chalkley, J. Cornfield, H. Park, *Science (80-.).* **1949**, *110*, 295.

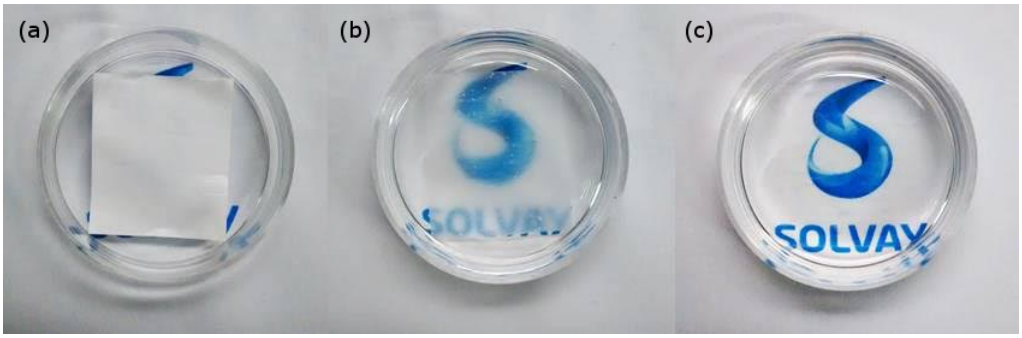

Figure 1. Images of a Hyflon AD® membrane. A fragment of membrane 5 (see Table 2) is shown after drying (a), and when soaked with ethanol (b) or water (c).

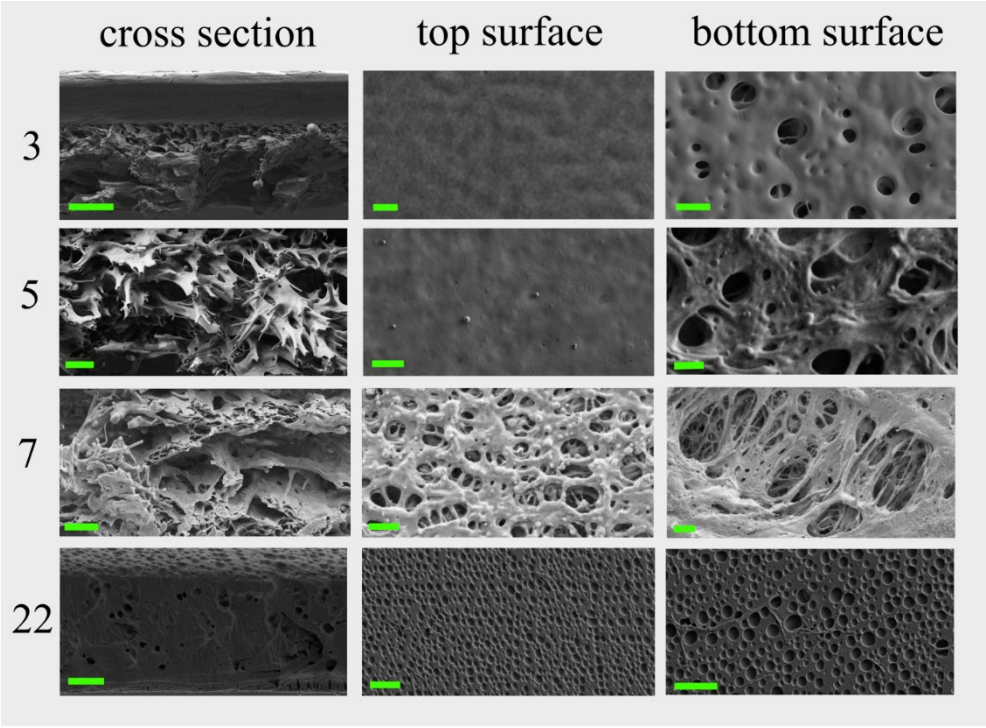

Figure 2. SEM images of Hyflon AD® membranes. Cross section (left), top surface (centre) and bottom surface (right) of membranes 3, 5, 7 and 22, as reported in Table 2. Scale bars represent 10 μm.

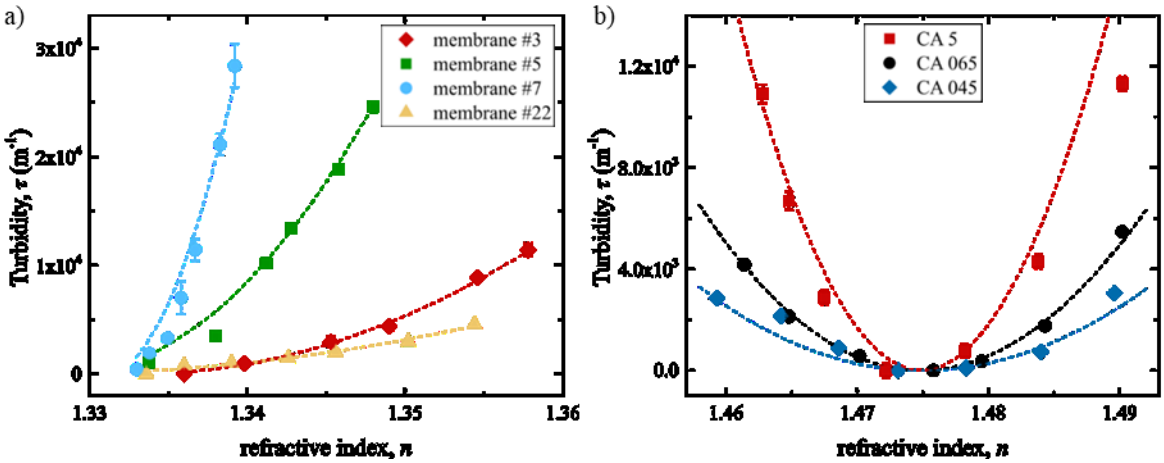

Figure 3. Turbidity of Hyflon AD® and CA membranes. a) Turbidity measured for membranes 3 (red diamonds), 5 (green squares), 7 (blue circles) and 22 (yellow triangles) as a function of solution refractive index varied by adding increasing amount of ethanol to water. b) Turbidity measured for CA045 (blue diamonds), CA065 (black circles) and CA5 (red squares) membranes as a function of solution refractive index varied by changing the fraction of p-cymene and isopropyl alcohol.

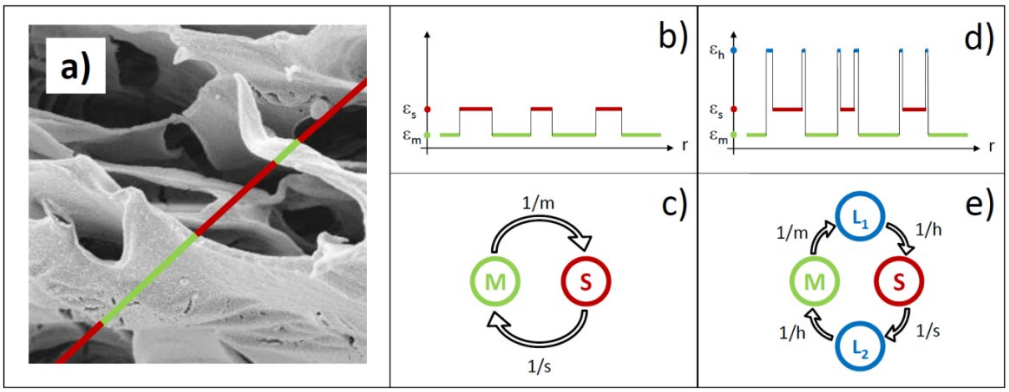

Figure 4. Schematic of RTS model. (a) SEM image of a Hyflon AD membrane and representation of a crossing ray with m and s segments, which are the chords of membrane and solution regions. (b) Example of dielectric constant values experienced by a ray crossing the membrane. (c) Two-state Markov model describing the continuous switch between the values of dielectric constant ε_m and ε_s experienced by a crossing ray. (d) Four-state Markov model describing the passage through a layer with dielectric constant ε_h at the interface between membrane and solution.

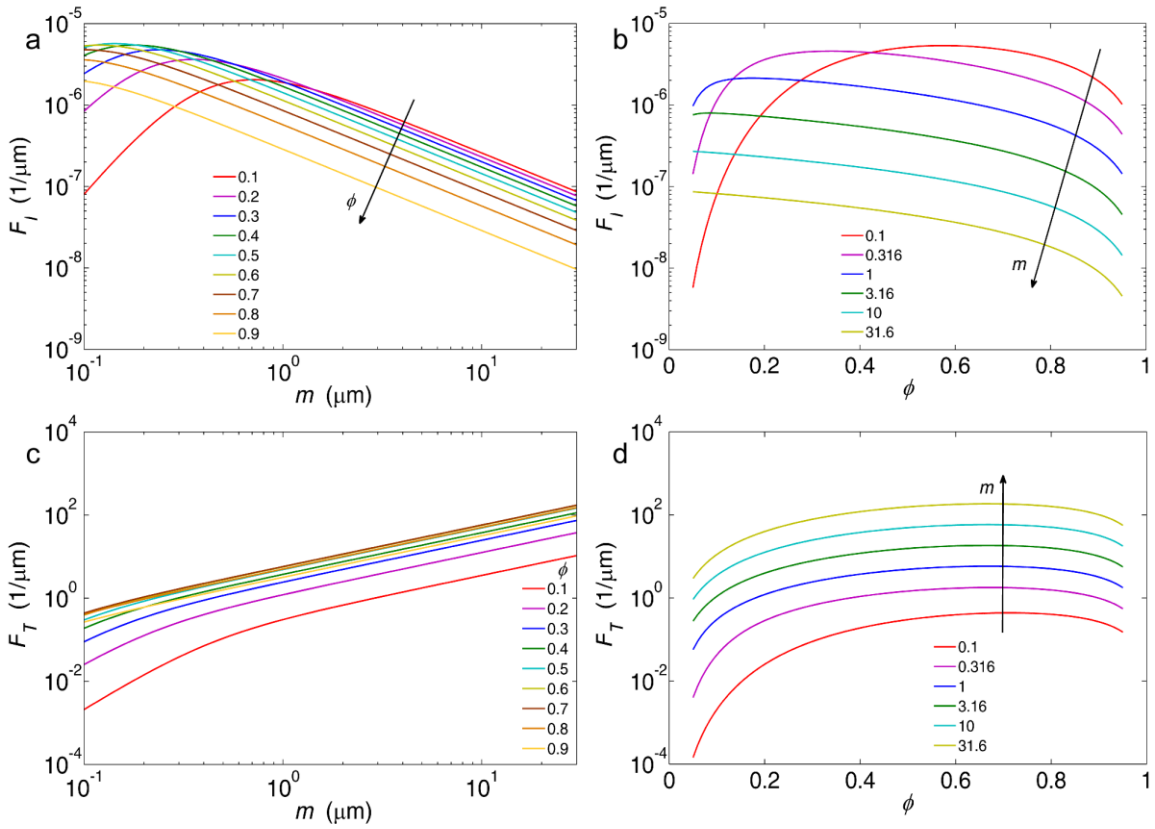

Figure 5. Scattered light intensity and turbidity calculated by two-state RTS model. Normalized intensity of scattered light computed by Equation (7) for $\theta = 30°$ as a function of the parameter m for various ϕ (a) and the parameter ϕ for various m (b). Normalized turbidity computed by Equation (8) as a function of the parameter m for various ϕ (c) and the parameter ϕ for various m (d). In all cases, $\lambda = 0.5$ μm.

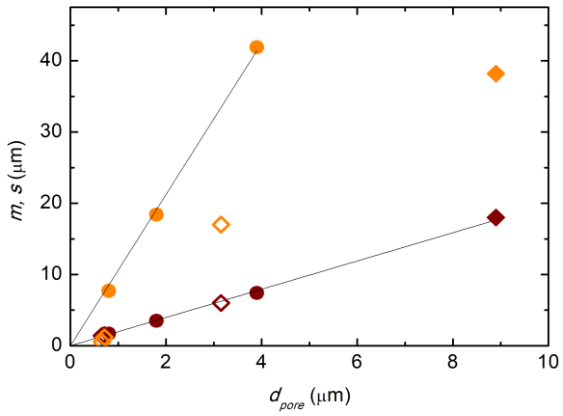

Figure 6. Dependence of chord lengths m and s on membrane filtering size. Values of m (brown symbols) and s (orange symbols) obtained from the fit of the dependence of τ on the solution refractive index for CA membranes (full circles) and Hyflon AD membranes (diamonds). For CA membranes and membrane 7 (full symbols), d_{pore} was measured by capillary flow porometry and the black lines are linear fits of s and m data for these membranes, respectively. For membranes 3, 22 and 5 (open diamonds), the value of d_{pore} has been extrapolated from the linear dependence of m extracted from the fit.

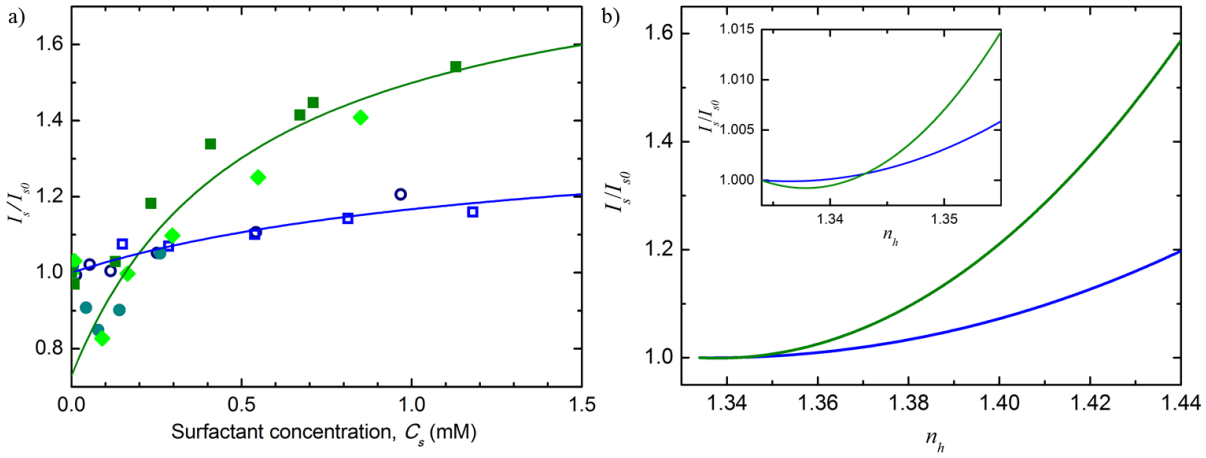

Figure 7. a) Relative increase of the scattering light intensity upon adsorption of surfactant. Measured scattered light intensity at $\theta = 30°$ upon addition of SBSAC surfactant in solution for membrane 5 (green full symbols) and 7 (blue open symbols). The data are taken after full equilibration of the scattering signal. Mixing of the sample after the addition of surfactant is provided by a magnetic stirring bar. Data points with different symbols and shades of the same color refer to repeated measurements. Continuous lines represent fits with equation $I_s/I_{s0} = a+b(1+C_{1/2}/C_s)^{-1}$. The parameters obtained from the fit of 7 data (blue line) are $a = 1$, $b = 0.39$, and $C_{1/2} = 1.34$ mM, those for 5 data with $C_s > 0.1$ mM (green line) are $a = 0.73$, b = 1.16, and $C_{1/2} = 0.53$ mM. b) Calculated dependence of scattered light as a function of the refractive index of an adsorbed layer. The dependence of I_s/I_{s0} on n_h is computed by Equation (16) using the parameters ϕ and m reported in Table 4 and a thickness h yielding I_s/I_{s0} equal to the maximum value reported in Figure 8. Blue: membrane 7, $\phi = 0.68$, $m = 18$ μm, $h = 14$ nm; green: membrane 5, $\phi = 0.74$, $m = 6$ μm, $h = 18.5$ nm. Inset: enlarged view at small value of h showing the local minimum.

Table 1. Preparation conditions explored for the production of Hyflon AD membranes.

	Preparation conditions						Membrane parameters	
# sample	Casting solvent	% wt of Hyflon AD	% wt of Cyclohexanone	Casting temperature	Coagulation bath acetone:ethanol	Washing step	Porosity [%]	Thickness [µm]
3	HFE7100	15	0	25	3:7	no	44	97
5	HFE7100	15	5	10	1:1	yes	74	92
7	HFE7100	15	5	10	1:1	yes[a)]	71	120
22	HFE7300	14	6	25	pure ethanol	no	28	25

[a)] An additional treatment was applied to open the pores at the membrane surface: the membrane was soaked for 15 minutes with a mixture of ethanol and 5% of HFE7100.

Table 2. Structural parameters of AC and Hyflon AD membranes.

Membrane	Porosity ϕ [%][a)]	m [µm][b)]	s [µm][b)]
CA045	82	1.7	7.7
CA065	84	3.5	18.4
CA5	85	7.4	41.9
3	44	1.5	1.2
5	74	6	17
7	68	18	38.2
22	28	1.4	0.54

[a)] ϕ was obtained from gravimetric porosity measurements. [b)] Chord lengths m and s were obtained from the analysis of the turbidity as a function of the refractive index of the solution.

Table of Contents (ToC)

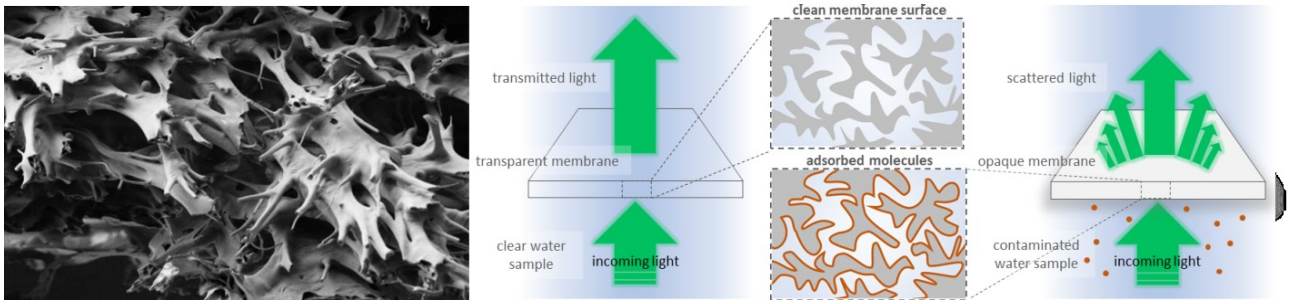

Perfluorinated microporous membranes with refractive index similar to that of water combine filtering and optical sensing capabilities. Their opacity is sensitive to the composition of the filling liquid and on the adsorption of molecular pollutants or foulants on the internal membrane surface. A simple model derived from the random telegraph signal accounts for the dependence of the optical response on the porosity and structure of different membranes.

ToC keyword: microporous membranes

Supporting Information

Fabrication and Optical Modelling of Micro-Porous Membranes Index-Matched with Water for On-Line Sensing Applications

Roberta Lanfranco, Fabio Giavazzi, Tommaso Bellini, Emanuele Di Nicolò & Marco Buscaglia[*]

S1. Solubility studies of Hyflon AD® 40

The solubility of Hyflon AD® was tested at different temperatures in four different solvents in order to find suitable conditions of polymer viscosity for casting. Physical properties of solvents are reported in **Table S1**. The hydrofluoroethers HFE 7100 [$C_2F_5CF(OCH_3)CF(CF_3)_2$] and HFE 7300 [$CH_3OCF_2CF(CF_3)_2$], both purchased from 3M, being partially fluorinated solvents and hence miscible with hydrogenated fluids, enabled the use of acetone or ethanol as non-solvent in the coagulation process. Galden SV90, gently provided by Solvay Specialty Polymers, and perfluorooctane [C_8F_{18}] (Sigma Aldrich) are fully fluorinated solvents, hence required the use of 1,3-bis(trifluoromethyl)benzene [$C_6H_4(CF_3)_2$] (Sigma Aldrich) as a (miscible) non-solvent. We investigated binary phase diagrams of Hyflon AD® and these solvents, instead of ternary phase diagrams, in order to better understand the best temperature-concentration window for casting and to easily explore the solubility limit.

Increasing concentrations of Hyflon AD®, from 5% to 30% wt, were dissolved in the selected solvents inside 10 mL glass tubes, mixed using a vortex and sonicated for 1 hour to dissolve the large powder aggregates. To study the solubility in temperature, the glass tubes were immersed in a thermic oil bath (Falc Bo Digit), starting from high temperature below the evaporation point of the solvent down to room temperature. Every 10 hours the mixtures were controlled by eyes, using tilting tube method [1] to verify the change of viscosity. Results of tilting tube tests performed at different polymer concentrations and temperatures are reported in **Figure S1**. At high polymer concentrations, Hyflon AD®–Galden SV90 samples underwent phase separation at any temperature, whereas at low polymer concentrations the samples were liquid, with an apparent viscosity similar

to that of water, hence unsuitable for casting. For this reason, we discarded Galden SV90 as possible casting solvent for membrane fabrication.

Table S1. Physical properties of casting solvents used for membrane fabrication.

Solvent	Boiling point [°C]	Partially hydrogenated[a)]	Liquid density [g ml^{-1}]^2	Viscosity [mPa s][b)]	Surface Tension [mN m^{-1}]^2
HFE 7100	61	yes	1.52	0.58	13.6
HFE 7300	98	yes	1.66	1.18	15
Galden SV90	90	no	1.69	1.13	16
Perfluorooctane	103	no	1.77	1.23	14

[a)]Among the four used fluorinated solvents, only HFE solvents being partially hydrogenated are miscible with alcohols and ketons; [b)]Density, viscosity and surface tension are given at 25 °C.

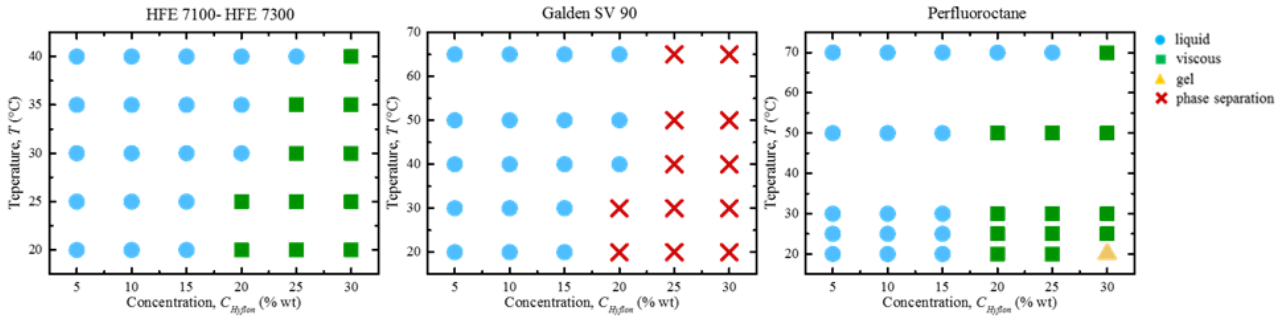

Figure S1. Solubility diagrams of Hyflon AD® in different solvents using tilting tube method. The solubility of Hyflon AD® in solvents HFE 7100 and HFE 7300 is found to be the same.

S2. Preparation conditions of Hyflon AD® membranes

Hyflon AD® membranes were produced as described in the Experimental section. Here we report all the explored experimental conditions for the preparation of flat sheet membranes and their measured thickness and porosity (**Table S2)**.

Table S2. Preparation conditions explored for the production of Hyflon AD® membranes.

	Preparation conditions	Membrane parameters

# sample	Casting solvent	% wt of Hyflon AD	% wt of Cyclohexanone	Casting temperature	Coagulation bath acetone:ethanol	Washing step	Porosity [%]	Thickness [μm]
1		13	0	25	3:7	no	48	57
2		13	0	25	pure ethanol	no	49	46
3		15	0	25	3:7	no	44	97
4		15	0	25	pure ethanol	no	50	98
5		15	5	10	1:1	yes	74	92
6		15	5	10	1:1	yes	68	66
7		15	5	10	1:1	yes + treatment 1[a)]	71	120
8	HFE7100	15	5	10	1:1	yes + treatment 2[a)]	72	104
9		15	5	10	1:1	yes + treatment 3[a)]	68	104
10		16	0	25	1:1	yes	66	58
11		17	0	25	3:7	no	60	103
12		17	0	25	pure ethanol	no	37	77
13		18	0	25	1:1	yes	70	64
14		18	5	25	1:1	yes	76	97
15		13	0	25	3:7	no	56	37
16		13	0	25	1:1	yes	53	51
17		14	4	25	pure ethanol	no	45	36
18		15	5	25	1:1	yes	64	61
19	HFE7300	15	5	10	1:1	yes	59	57
20		14	0	25	pure ethanol	no	36	35
21		14	2	25	pure ethanol	no	47	44
22		14	6	25	pure ethanol	no	28	25
23		16	0	25	1:1	yes	52	46

[a)] An additional treatment was applied to open the pores at the membrane surface: the membranes were soaked for 15 minutes with a mixture of ethanol and 5% (treatment 1), 10% (treatment 2) or 15% (treatment 3) of HFE7100.

S3. Standard methods for membrane characterization

S2.3.1. Thickness

Membrane thickness was measured by using a digital micrometer (model ID-H0530, Mitutoyo, Japan), with a precision of ±0.001 mm. Thickness was measured in at least 5 different regions of the membrane and the average value was considered.

S2.3.2. Gravimetric porosity

Membrane porosity ϕ was determined according to the gravimetric method. Porosity is defined as the ratio between the volume of voids and the total volume occupied by the membrane. Perfectly dry membrane pieces were weighed and impregnated with liquid using isopropylic alcohol for Hyflon AD® membranes and water for CA membranes. After 24h, the excess of the liquid was removed with tissue paper, and membranes weight was measured again. Finally, from the dry (w_{dry}) and the wet weight (w_{wet}) of the sample, the porosity of the membrane was obtained using the following formula:

$$\phi = \frac{\frac{w_{wet}-w_{dry}}{\rho_l}}{\frac{w_{wet}-w_{dry}}{\rho_l}+\frac{w_w}{\rho_p}} \quad \text{(S1)}$$

where ρ_w is either the density of isopropylic alcohol (0.78 g cm^{-3}) or water (0.997 g cm^{-3}) and ρ_p is the Hyflon AD® density (1.98 g cm^{-3}) [2] or CA density (1.28 g cm^{-3}). For all membrane types, at least three measurements were performed; then, average values and corresponding standard deviations were calculated.

S2.3.3. Pore size

Pore size distribution and bubble point tests were both performed by capillary flow porometry using a Porolux TM 1000 (Porometer NV, Belgium).[3] This test was performed on CA membranes and on three Hyflon AD® membranes with both surface open enough to enable flow measurements (sample 7, 8 and 9). A 1 cm^2 disc of membrane sample was soaked with a wetting liquid (isopropyl alcohol for Hyflon AD® membrane and water for CA membranes) for 24h, then an increasing nitrogen pressure was applied to force the wetting liquid out of through-pores. In a range of small applied pressures no flow through the membrane was observed due to capillary forces. Then, a flow was observed when the largest pores were emptied, hence defining the so-called "bubble point" pressure. The pressure was gradually increased to empty all pores and then the volumetric flow is measured. After this “wet” run (down-facing triangles in Figure S2), a “dry” run (up-facing

triangles) was performed while gradually reducing the pressure. The pore size was calculated using Washburn equation.[4] The pore sizes d_{pore} obtained by this test are reported in **Table S3**.

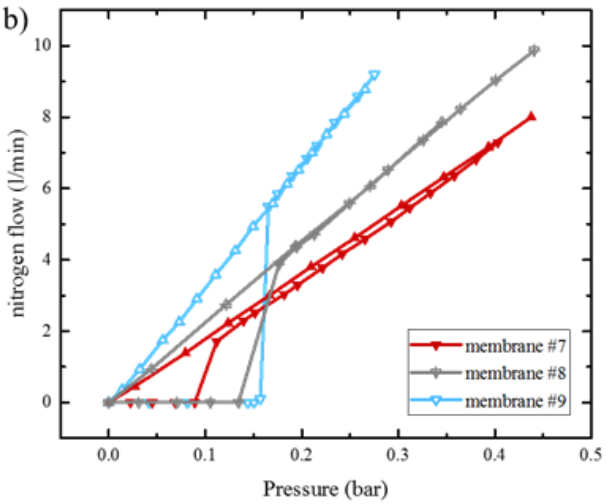

Figure S2. Capillary flow porometry characterization of three Hyflon AD® membrane samples presenting open surfaces. Flow of nitrogen passing through the membrane is measured as a function of the applied pressure (down-facing triangles for "wet" run and up-facing triangles for "dry" run).

Table S3. Pore size measured by capillary flow porometry.

Membrane	Smallest pore [µm]	Mean pore, d_{pore} [µm]	Bubble point pore [µm]
CA045	0.43	0.78	2.24
CA065	1.76	1.83	1.76
CA5	2.24	3.92	5.23
7	2.14	8.91	8.2
8	3.47	5.67	4.92
9	5.23	5.36	5.23

S2.3.4. Scanning Electron Microscope (SEM) imaging

Scanning Electron Microscope (SEM) images were taken using a Leo-Zeiss Supra 35, with a Field Emission Gun (Schottky type). Prior to SEM measurements, the samples were dried, broken in liquid nitrogen and finally sputtered with a thin layer of gold in order to make them conductive. SEM images of Hyflon AD® 40 membrane samples are reported in Figure 2 in the main text.

S2.3.5. Thermal gravimetric analysis

Thermal gravimetric analysis (TGA) measurements were performed using a Perkin Elmer instrument (Perkin Elmer 8000) using a 10 °C min^{-1} ramp in air.[5] This technique was used to assess the amount of residual solvent present in the membranes previously dried under fume hood for several days. In this technique, the loss in weight of a membrane sample is monitored while it is heated from room temperature up to 450 °C. The normalized weight of three membrane samples, two made using solvent HFE7100 (sample 5 and 10) and one using HFE7300 (sample 19), are reported in **Figure S3**. Sample 5, produced with HFE7100 and 5% of cyclohexanone, provides a loss in weight of 1.1%, smaller than the other samples.

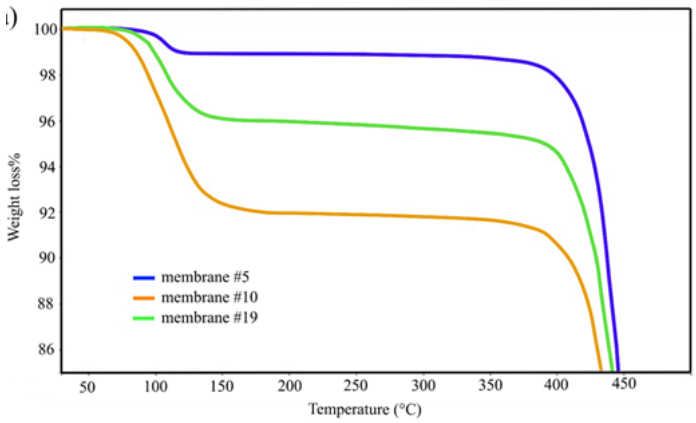

Figure S3. TGA experiments to measure the amount of residual solvent in Hyflon AD® membranes. The first drop is due to evaporation of trapped solvent in the membrane, while the second is due to degradation of the polymer itself.

S4. Measurements of light scattered by the membranes

A custom optical set-up was built to measure the intensity of light scattered by the membranes for different composition of the soaking solution and for different concentrations of surfactant adsorbing on the internal membrane surface. The instrument allows the simultaneous measurements of scattered light at a fixed angle and transmitted light, from which the sample turbidity is obtained.

As shown in **Figure S4a**, the set-up is composed by a green diode laser (λ= 532 nm, Coherent Compass 315M-100), a spatial filter, and a thermostatic cell holder. The measuring cell is made of a square quartz cuvette and a rectangular custom-made frame made of poly(methyl methacrylate) or PTFE, holding 5 x 10 mm membrane samples (**Figure S4b**). The mixing of the solution inside the measuring cell was provided by a magnetic stirring bar. The scattering signal at fixed angle $\theta = 30°$ relative to the direction of the transmitted light is collected using a multimode optical fibre. The instrument also enables the acquisition of light intensity transmitted by the sample through spatial filtering, hence enabling the measurement of the sample turbidity τ, which represents the total scattering cross section per unit volume of material. The transmitted light beam is focused by a lens on a pinhole of 50 μm in diameter to collect only light rays that are not scattered or deflected crossing the membrane. According to the Lambert-Beer law, the light intensity I_T that passes through the membrane decreases with the thickness d as $I_T/I_0 = e^{-\tau d}$, where I_0 is the incident light intensity. Thus, the turbidity is measured as:

$$\boldsymbol{\tau = -\frac{1}{d} log\left(\frac{I_T}{I_0}\right)} \qquad \text{(S2)}$$

The refractive index of the solution soaking the membrane was changed by mixing ethanol and water, in the case of Hyflon AD® membranes, or p-cymene [$C_{10}H_{14}$] and isopropyl alcohol, for matching the refractive index of CA filters. The refractive index of the solutions was measured by an Abbe refractometer. In order to ensure a complete wetting of the pores of the Hyflon AD® membranes, all membranes were stored in a water/ethanol 1:1 mixture for at least a week and brought to the final solution four hours before the optical measurements.

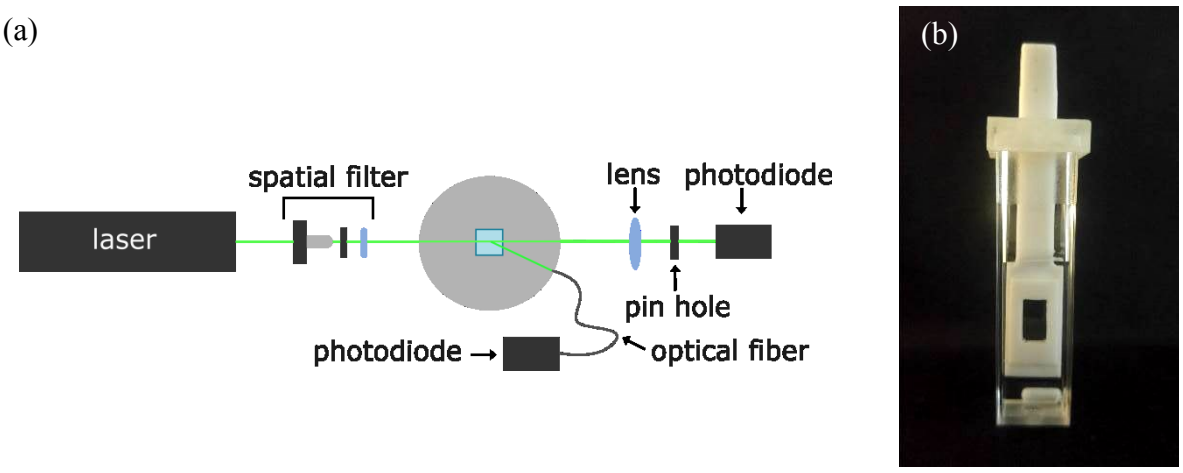

Figure S4. (a) Instrument for light scattering measurement. Schematic drawing of the optical set-up for the measurement of the intensity of scattered light at fixed angle and of the optical turbidity, obtained from the measurement of the transmitted light according to Equation (S2). (b) Picture of the custom-made membrane holder. A PTFE frame holds a membrane fragment with size at least 5 mm x 10 mm. The frame is immersed into a 1-cm spectroscopic cuvette containing a magnetic stirring bar for efficient mixing of the solution.

S5. Optical model for light scattered by a porous membrane in quasi index-matching conditions

In the Rayleigh-Gans regime, the intensity of scattered light I_s depends on the amplitude and size distribution of the fluctuations of dielectric constant inside the heterogeneous membrane-fluid medium as:[6]

$$\boldsymbol{I_s = \frac{I_0 k^4}{16\pi^2 R^2 \langle \varepsilon \rangle^2} |\mathcal{F}|^2} \qquad \text{(S3)}$$

where I_0 is the incident intensity, $k=2\pi/\lambda$, λ is the wavelength, $\langle \varepsilon \rangle$ is the average dielectric constant, R is the distance between the scattering volume and the observer, and

$$\boldsymbol{\mathcal{F} = \int_V \delta\varepsilon(r) e^{iq \cdot r} dV}. \qquad \text{(S4)}$$

Equation (S4) represents the sum of the contributions of all the elementary scattering elements to the total electric field, where $\delta\varepsilon(r) = \varepsilon(r) - \langle \varepsilon \rangle$ is the fluctuation of the dielectric constant from the

average value $\langle\varepsilon\rangle$, $q = 2k\langle\varepsilon\rangle^2\sin(\theta/2)$ is the modulus of the scattering vector and V is the scattering volume. The turbidity τ is obtained from integration of I_s in all direction:

$$\boldsymbol{\tau} = \frac{\int \boldsymbol{I_s R^2 d\Omega}}{\boldsymbol{I_0 V}} \tag{S5}$$

where $d\Omega$ is the solid angle element. The quantity $\boldsymbol{|\mathcal{F}|^2}$ is computed as described in the main text. Briefly, the dielectric constant inside the porous medium alternatively assumes one of two characteristic values, those of solution (ε_s) and membrane (ε_m). This transition happens randomly with a statistics that depends on two characteristic lengths (s and m) that describe the internal structure of the microporous membrane. The distances between two consecutive transitions are assumed statistically independent random variables. Here the intensity of scattered light I_s is computed from the parameters ε_s, ε_m, s and m treating the dielectric constant fluctuations as a Random Telegraph Signal (RTS).

The RTS model represents one of the simplest approach in electronics to describe shot noise or burst noise.[7][8] In optics, similar models have been previously used to compute the waves scattered by random media assuming rectangular corrugations on an incident wavefront,[9] and to describe dynamic light scattering of granular systems.[10] An approach similar to that developed here has been first proposed by Debye to model the small angle x-ray scattering from porous media.[11] More generally, the chord length distribution can be considered as a fundamental descriptor of the structure of two-phase systems.[12] Here we exploit the RTS model to derive the spatial correlation function of the dielectric constant fluctuations $\langle\delta\varepsilon(r)\delta\varepsilon(r+dr)\rangle$ at optical wavelength. Notably, since the function $\boldsymbol{\mathcal{F}}$ in Equation (S4) corresponds to the Fourier transform of $\delta\varepsilon(r)$, its square modulus $\boldsymbol{|\mathcal{F}|^2}$ can be obtained as the Fourier transform of the autoconvolution of $\delta\varepsilon(r)$, *alias* the spatial correlation function of the dielectric constant fluctuations $\langle\delta\varepsilon(r)\delta\varepsilon(r+dr)\rangle$:

$$\boldsymbol{|\mathcal{F}(q)|^2 = \langle|\delta\varepsilon(q)|^2\rangle} \tag{S6}$$

In the framework of RTS, the expression for the spatial correlation function of the dielectric constant fluctuations $\langle \delta\varepsilon(r)\delta\varepsilon(r+dr)\rangle$ is derived by the conditional probabilities of starting from a medium (membrane or solution) at position r and finding the same or the other medium at a distance dr. The calculation can be performed considering an equivalent two-state kinetic model, where the time coordinate is replaced by the space r and the characteristic rates are $1/m$ and $1/s$, respectively (Figure 4c). The model provides a correlation function decaying exponentially with a space constant $\gamma = (1/m+1/s)$. The amplitude is obtained considering that the correlation function for $dr = 0$ simply becomes $\langle \delta\varepsilon(r)^2\rangle$. Therefore, the resulting equation of the correlation function is remarkably simple:

$$\langle \boldsymbol{\delta\varepsilon(r)\delta\varepsilon(r+dr)}\rangle = \frac{\boldsymbol{ms}}{\boldsymbol{(m+s)^2}}(\boldsymbol{\varepsilon_s - \varepsilon_m})^{\boldsymbol{2}}\boldsymbol{e^{-\gamma r}} \qquad \text{(S7)}$$

The term $|\boldsymbol{\mathcal{F}}|^{\boldsymbol{2}}$ is computed from the Fourier transform of Equation (S7), and the scattered intensity and the turbidity are obtained from Equation (S3) and (S5).

This approach can be generalized to systems composed by any number of materials with different values of dielectric constant. When a thin layer with thickness h and having a different refractive index from the substrate and the soaking liquid is added on the internal surface of the membrane, the autocorrelation function of $\delta\varepsilon(r)$ is derived from an equivalent four-state kinetic system continuously cycling through the sequence of dielectric constant states $\varepsilon_m \rightarrow \varepsilon_h \rightarrow \varepsilon_s \rightarrow \varepsilon_h \rightarrow \varepsilon_m \ldots$. Similarly to the calculation performed for the two-state RTS model, the transition rates are given by $1/m$, $1/s$ and $1/h$, where h is much smaller than m and s. With this approximation, only two non-degenerate rates are obtained from the model: $\gamma = (1/m+1/s)$ and $\gamma_h = 1/h$. Therefore, the spatial correlation function of the dielectric constant fluctuations $\langle \delta\varepsilon(r)\delta\varepsilon(r+dr)\rangle$ is written as the sum of two exponential decays with rates γ and γ_h. The corresponding amplitudes of the exponential components are obtained considering the limit for $dr = 0$, in which the correlation function equals

$$\boldsymbol{a_0} = \langle \boldsymbol{\delta\varepsilon(r)^2}\rangle = \frac{\boldsymbol{m\delta\varepsilon_m^2+2h\delta\varepsilon_h^2+s\delta\varepsilon_s^2}}{\boldsymbol{m+2h+s}} \qquad \text{(S8)}$$

and for $h << dr_h << m$ and s, where the correlation function is computed as

$$\boldsymbol{a_h} = \langle \boldsymbol{\delta\varepsilon(r)\delta\varepsilon(r + dr_h)} \rangle = \frac{\boldsymbol{m\delta\varepsilon_m^2 + h\delta\varepsilon_h(\delta\varepsilon_m + \delta\varepsilon_s) + s\delta\varepsilon_s^2}}{\boldsymbol{m + 2h + s}}. \quad \text{(S9)}$$

Accordingly, the correlation function of the dielectric constant fluctuations is given by

$$\langle \boldsymbol{\delta\varepsilon(r)\delta\varepsilon(r + dr)} \rangle = \boldsymbol{(a_0 - a_h)e^{-\gamma_h r} + a_h e^{-\gamma r}}. \quad \text{(S10)}$$

Analogously to the two-state RTS model, the term $\boldsymbol{|\mathcal{F}|^2}$ is obtained from the Fourier transform of Equation (S10) and substituting into Equation (S3) and (S5) the intensity of scattered light and the turbidity can be recovered.

We computed the ratio between the scattered intensity I_s in the presence of the layer h and the intensity I_{s0} scattered by the bare membrane surface ($h = 0$) as:

$$\frac{\boldsymbol{I_S}}{\boldsymbol{I_{s0}}} = \boldsymbol{1} + \frac{\boldsymbol{h}}{\boldsymbol{m\phi}} \frac{\left((2\boldsymbol{\phi} - 1)n_h^2 + (\boldsymbol{\phi} - 1)n_m^2 + (2 - 3\boldsymbol{\phi})n_s^2\right)}{\left(n_m^2 - n_s^2\right)} + \boldsymbol{h^4} \frac{\left(\gamma^2 + q^2\right)^2 (2n_h^2 - n_m^2 - n_s^2)(n_h^2 + (\boldsymbol{\phi} - 1)n_m^2 - \boldsymbol{\phi} n_s^2)}{\left(n_m^2 - n_s^2\right)^2} \quad \text{(S11)}$$

that for $n_s \approx n_m$ is well approximated by

$$\frac{\boldsymbol{I_S}}{\boldsymbol{I_{s0}}} = \boldsymbol{1 + h\gamma(1 - 2\phi)N_1 + 2h^4(\gamma^2 + q^2)^2 N_1^2} \quad \text{(S12)}$$

where

$$\boldsymbol{N_1} = \frac{(n_h^2 - n_s^2)}{(n_s^2 - n_m^2)} \approx \frac{\boldsymbol{1}}{\boldsymbol{N_0}} \left(\frac{n_h^2}{n_s^2} - \boldsymbol{1}\right) \quad \text{(S13)}$$

According to Equation (S13), the linear term in h is negative for $\phi > 0.5$ if $n_s > n_m$, hence providing an initial small decrease of the scattered light intensity with the growth of parameter h followed by an increase as h^4. Similarly, a local minimum of scattered intensity at the initial stage of coating was previously observed for a system of dispersed nanoparticles index matched with water.[13]

S6. Chord lengths and filtering pore size for regular periodic structures

Model periodic structures were simulated in order to investigate the scaling between void volume fraction ϕ, filtering pore size d_{pore}, chord lengths of solution s and membrane m. Three kinds of

structures were investigated on a square periodic lattice: (i) a cubic frame structure with variable thickness of the frame (Figure S5b); (ii) a cube with a centred spherical void volume of variable radius (Figure S5d); (iii) and empty cube with circular apertures of variable diameter (Figure S5f). Structures (i) and (ii) are defined by one single parameter related to the void fraction ϕ, whereas structure (iii) is also defined by the aperture diameter, which basically indicates d_{pore}. A Matlab program was used to compute the statistics of random rays passing through the simulated periodic structures. For each structure a binary cubic cell with edges of length 300 bits was generated, where the binary digit represents the solution or membrane volume element. Starting from a random position and with a random orientation each time, 10.000 rays traveling straight for 3000 bits each were considered. The parameters s and m were computed as the average lengths of uninterrupted solution and membrane stretches, respectively. In all cases, the volume fraction ϕ of the solution binary elements was confirmed to be given by $\phi = s/(s+m)$. For all structures, the value of m decreases with ϕ. In the case of structure (i) and (ii), both s and d_{pore} increase with ϕ. In contrast, in structure (iii) both s and d_{pore} are almost insensitive to ϕ. Indeed, in this structure s and m are substantially independent from the aperture diameter, whereas d_{pore} is independent from ϕ. This study suggests that the values of chord lengths s and m accessible through the measurement of light scattering intensity can be independent from the value of d_{pore} measured by capillary flow porometry. Both approaches provide insights on the overall membrane structure.

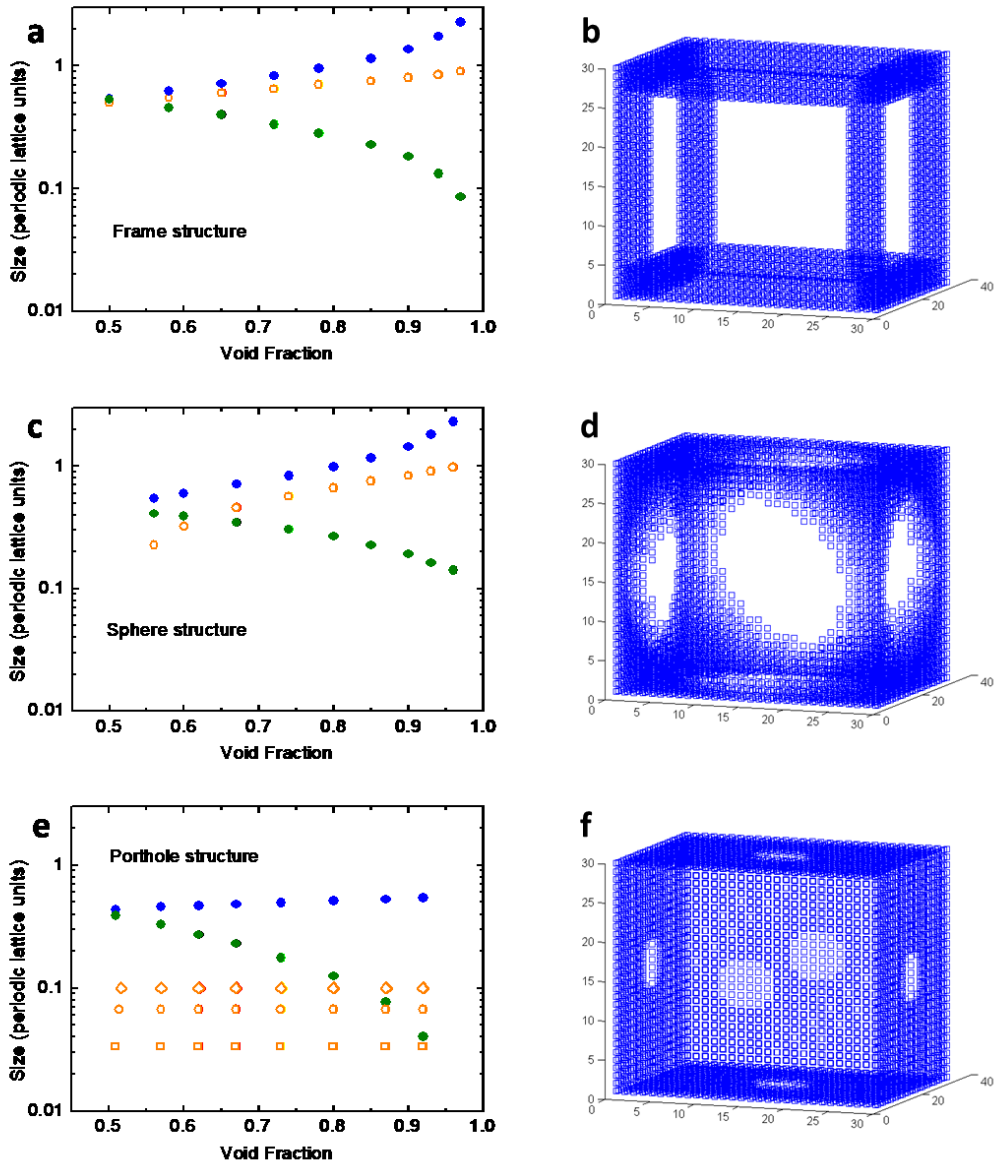

Figure S5. Chord lengths analysis of model structures. (a),(c), and (e) report the average s values (blue), m values (green) and minimum pore diameter d_{pore} (orange) as function of void volume fraction ϕ for different periodic structures: (a),(b) cubic frame structure; (c),(d) spherical void into cubic lattice; (e),(f) holes into empty cubic structure. In (b),(d) and (f) the blue regions represent the membrane volume. In (e), orange diamonds, circles and squares represent different choices of aperture diameter, all yielding similar s and m values.

References

[1] B. J. Cha, J. M. Yang, *J. Memb. Sci.* **2007**, *291*, 191.

[2] X. Li, Y. Wang, X. Lu, C. Xiao, *J. Memb. Sci.* **2008**, *320*, 477.

[3] D. Li, M. W. Frey, Y. L. Joo, *J. Memb. Sci.* **2006**, *286*, 104.

[4] E. W. Washburn, *Phys. Rev.* **1921**, *17*, 273.

[5] C. Joly, D. Le Cerf, C. Chappey, D. Langevin, G. Muller, *Sep. Purif. Technol.* **1999**, *16*, 47.

[6] H. C. van de Hulst, *Light Scattering by Small Particles*, Dover, New York, **1957**.

[7] S. O. Rice, *Bell Syst. Tech. J.* **1944**, *23*, 282.

[8] S. Machlup, *J. Appl. Phys.* **1954**, *25*, 341.

[9] E. Jakeman, E. Renshaw, *J. Opt. Soc. Am. A* **1987**, *4*, 1206.

[10] P.-A. Lemieux, D. J. Durian, *Appl. Opt.* **2001**, *40*, 3984.

[11] P. Debye, H. R. Anderson, H. Brumberger, *J. Appl. Phys.* **1957**, *28*, 679.

[12] W. Gille, *Eur. Phys. J. B* **2000**, *17*, 371.

[13] D. Prosperi, C. Morasso, F. Mantegazza, M. Buscaglia, L. Hough, T. Bellini, *Small* **2006**, *2*, 1060.